Nuclear Instruments and Methods in Physics Research A 833 (2016) 8–14

Contents lists available at ScienceDirect

Nuclear Instruments and Methods in Physics Research A

journal homepage: www.elsevier.com/locate/nima

Analysis and comparison between electric and magnetic power couplers for accelerators in Free Electron Lasers (FEL)

C. Serpico [a,*], A. Grudiev [b], R. Vescovo [c]

[a] Elettra - Sincrotrone Trieste, Trieste, Italy
[b] CERN, Geneva, Switzerland
[c] University of Trieste, Trieste, Italy

ARTICLE INFO

Article history:
Received 20 May 2016
Received in revised form
15 June 2016
Accepted 28 June 2016
Available online 1 July 2016

Keywords:
RF Coupler
High gradient
Multipole fields
FEL

ABSTRACT

Free-electron lasers represent a new and exciting class of coherent optical sources possessing broad wavelength tunability and excellent optical-beam quality. The FERMI seeded free-electron laser (FEL), located at the Elettra laboratory in Trieste, is driven by a 200 m long, S-band linac: the high energy part of the linac is equipped with 6 m long backward traveling wave (BTW) structures. The structures have small iris radius and a nose cone geometry which allows for high gradient operation. Development of new high-gradient, S-band accelerating structures for the replacement of the existing BTWs is under consideration. This paper investigates two possible solutions for the RF power couplers suitable for a linac driven FEL which require reduced wakefields effects, high operating gradient and very high reliability. The first part of the manuscript focuses on the reduction of residual field asymmetries, while in the second analyzes RF performances, the peak surface fields and the expected breakdown rate. In the conclusion, two solutions are compared and pros and cons are highlighted.

1. Introduction

Linac driven Free-Electron lasers generate tunable, Fourier-transform-limited, femtosecond duration X-ray pulses, thus providing an investigation tool of fundamental importance for present-day science. Such pulses enable time and frequency-resolved dichroic scattering experiments, electron emission spectroscopy and coherent-pulse-based spectroscopy [1–3].

However, the ultimate photon beam performance necessary to produce such pulses, results in demanding requirements on the electron beam quality, in terms of both emittance and longitudinal phase space flatness [4]. Longitudinal and transverse wakefields worsen the beam quality and eventually lead to an undesired emittance growth.

FERMI is a seeded free-electron laser, operating in the VUV to soft X-rays range, driven by a 200 m long, S-band linac. The high energy part of the linac is equipped with seven, 6 m long backward traveling wave (BTW) structures. The structures have small iris radius and a nose cone geometry which allows for gradients up to 26 MV/m. Nonetheless, such a small iris radius bring significant longitudinal and transverse wakefields effects, important in particular at high bunch charges. Furthermore, BTWs have been found to suffer from increased breakdown activity when operated at the maximum gradient with a 50 Hz repetition rate.

As a user facility, the highest reliability must be guaranteed even when operated at the ultimate limit. Therefore development of new, low wakefields, high gradient and high reliability S-band accelerating structures for the replacement of the existing BTWs is under consideration.

The following paper examines possible solutions for the RF power couplers for the new structures. As confirmed by recent experimental results with X-band accelerator structures [5,6], RF power couplers, where the energy is transferred between the cavity and connecting waveguides, is the region most prone to RF breakdown and surface degradation. Furthermore, electric and magnetic field asymmetries (i.e. dipole and quadrupole kick components) in the coupler region can induce an head–tail kick on the e-beam, causing an unacceptable emittance degradation.

Standard couplers connect the feed waveguide directly to the equator of the end-cell through a magnetic coupling slot, while waveguide couplers couple the power to the structure axially [7–9].

After an introduction to the field asymmetries and the quadrupole kick in the RF couplers, a comparison between a dual feed magnetic-coupled RF coupler (i.e. MC-coupler) and a dual-feed electric-coupled RF coupler (i.e. EC-coupler) is presented. In particular, the residual electric and magnetic field asymmetries are minimized as well as high surface fields that might limit the achievable accelerating gradient.

* Corresponding author.
E-mail address: claudio.serpico@elettra.eu (C. Serpico).

http://dx.doi.org/10.1016/j.nima.2016.06.131
0168-9002/

2. Field asymmetry analysis

Field asymmetries in the coupler cell and the minimization of the residual quadrupole components have been widely studied in the past years [10,11,9,12].

While providing good matching, the coupling slots may in fact produce non-axial-symmetric field distribution in the coupler region. As stated above, the residual asymmetries can worsen beam quality and bring to undesired emittance growth. This is particularly detrimental for low emittance beams at low energies and in the injector accelerators for light sources. The present paragraph will recall analytic formulae obtained in referenced papers. Such formulae will then be used in the sequel to calculate and compare residual field asymmetries in two different types of RF couplers.

The actual impact on the electron beam dynamics produced by field asymmetries in the coupler region can be studied by analyzing the transverse momentum change experienced by the particles passing through the RF coupler.

A particle of charge q, moving with velocity $\vec{v}$ through an electromagnetic field, experiences the Lorentz force:

$$\vec{F} = q\left[\vec{E} + \vec{v} \times \vec{B}\right] \tag{1}$$

where $\vec{E}$ is the electric field and $\vec{B}$ is the magnetic flux density acting on the particle.

For an ultra-relativistic particle of charge q and momentum p, passing through an RF quadrupole, the transverse kick is given by:

$$\Delta\vec{p}_{\perp} = pk_2\left(x\hat{u}_x - y\hat{u}_y\right)\cos\omega t \tag{2}$$

where ω is the operating angular frequency, $\hat{u}_x$ and $\hat{u}_y$ are the unit vectors of the x- and y-axis respectively, and k_2 is the amplitude of the normalized integrated quadrupolar strength [11].

The focusing strength of the quadrupolar field can be calculated by Eq. (3); the corresponding defocusing strength is instead calculated according to Eq. (4)

$$k_{2,x} = \frac{q}{pc}\frac{1}{\pi r}\int_0^{2\pi}\left\|\int_0^L F_x(r,\varphi,z)e^{j\frac{\omega z}{c}}dz\right\|\cos\varphi d\varphi \tag{3}$$

$$k_{2,y} = \frac{q}{pc}\frac{1}{\pi r}\int_0^{2\pi}\left\|\int_0^L F_y(r,\varphi,z)e^{j\frac{\omega z}{c}}dz\right\|\sin\varphi d\varphi \tag{4}$$

Eqs. (3) and (4), (r,φ,z) are given in circular cylindrical coordinates, as shown in Fig. 1, F_x and F_y are the x- and y-components, respectively, of the Lorentz force, and c is the velocity of light.

For any ideal quadrupole, $k_{2,x} = -k_{2,y}$. In particular, along the line (r, $\varphi = 45°$, z=constant) (see Fig. 1), the components of the Lorentz force along the x- and y-axes are equal.

Due to the symmetry of the dual feed coupler setup, certain multipolar components cannot be excited in the structure: dipolar, sextupolar, etc. are not allowed. Nonetheless, there is a residual octupolar component in addition to the quadrupolar one. In order to fully evaluate the residual field asymmetries in the coupler region, the following function $F_\varphi(z)$ is introduced:

$$F_\varphi(z) = \left[F_x(r = 5\text{ mm}, \varphi = 45°, z) - F_y(r = 5\text{ mm}, \varphi = 45°, z)\right] \tag{5}$$

This function is integrated along a line of length L, contained in the coupler region, parallel with the z-axis and specified by the cylindrical coordinates $r = 5\,mm$ and $\varphi = 45°$. This yields the quantity:

$$k_q = \frac{1}{qr}\left|\int_0^L F_\varphi(z)e^{\pm j\frac{\omega}{c}z}dz\right| \tag{6}$$

In Eq. (6), the factor $e^{\pm j\frac{\omega}{c}z}$ takes into account the transit time effect, while the propagation velocity of the wave in the z-direction is intrinsic in the z-dependence of the phase of $F_\varphi(z)$.

The values of k_q are also normalized to r in order to obtain a quantity that is no longer dependent on r (the integrand function is linear with respect to r).

3. Magnetic-coupled RF coupler

The radio frequency power is transferred from a rectangular waveguide to an accelerating structure (operating on the TM_{01} mode) through a slot aperture between the wall of the rectangular waveguide and the coupling cell. In this case, the magnetic field in the waveguide is coupled to the magnetic field lines in the coupling cell [8,13].

The RF coupler is matched to the accelerating structure by adjusting both the slot aperture and the radius of the coupling cell (respectively a and r in Fig. 2). The coupling slot introduces a distortion in the field distribution, resulting in multi-pole field components which affect the beam dynamics. Using symmetric feeding, with two input waveguides on opposite sides of the coupling cell as indicated in Fig. 3, the odd magnetic field components are suppressed, but there could still be even components like quadrupoles, octupoles, etc. [13].

A racetrack profile of the coupler cell reduces the residual quadrupole component of the field [14,15] by optimizing the distance d between the two half-circles, as shown in Fig. 3.

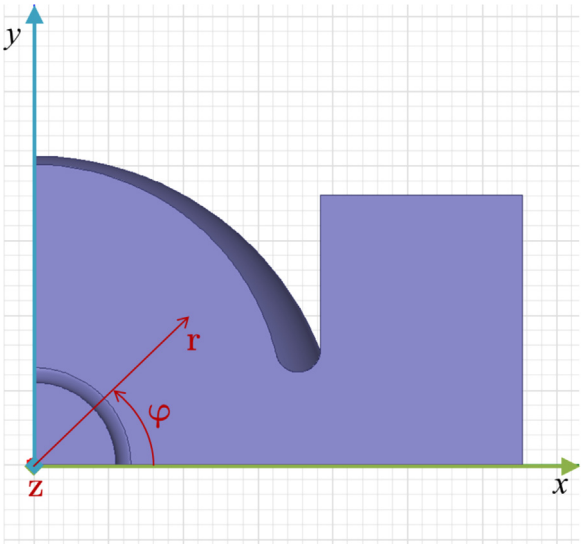

Fig. 1. Transverse section of the structure and circular cylindrical coordinates.

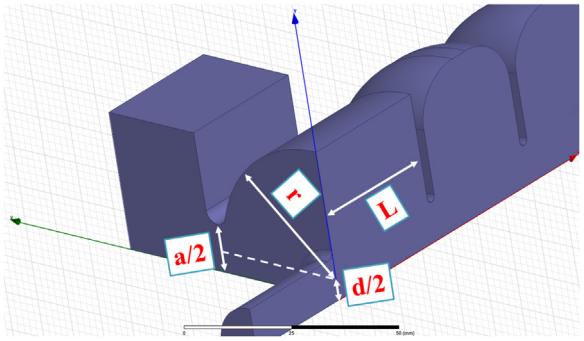

Fig. 2. Geometrical parameters for the magnetic coupled RF coupler: a is the coupling slot aperture, d is the racetrack parameter and r is the coupling cell radius.

In our case, the length of the coupler cell L is 34.036 mm (Fig. 3), exactly matching the short dimension of a WR284 rectangular waveguide. The residual quadrupole component has been calculated [16] as a function of the racetrack parameter d.

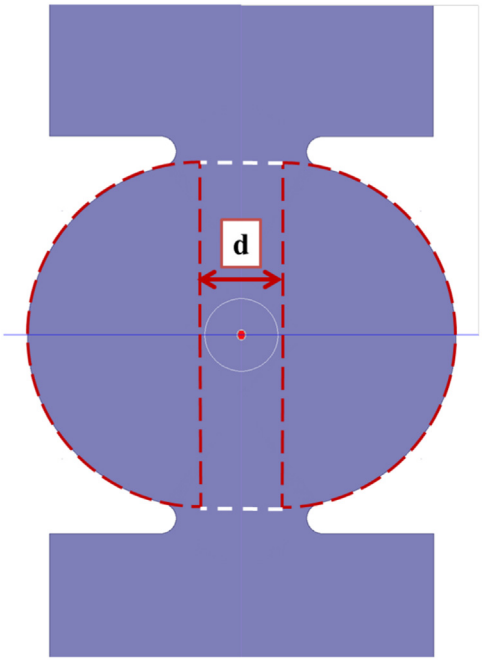

Fig. 3. Racetrack profile for the magnetic coupled RF coupler.

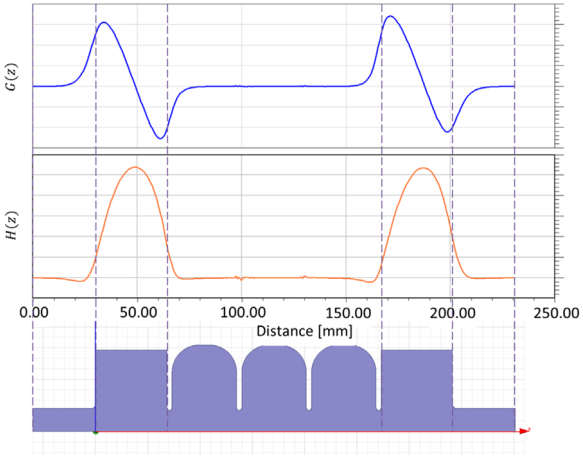

Fig. 4. Plot of $G(z)$ and $H(z)$, the real and the imaginary parts of the integrand function in Eq. (6).

Fig. 4 shows a plot of $G(z) = \Re\left[F_\varphi(z)e^{\pm j\frac{\omega}{c}z}\right]$ and $H(z) = \Im\left[F_\varphi(z)e^{\pm j\frac{\omega}{c}z}\right]$, respectively the real and the imaginary parts of the integrand function of Eq. (6) for a structure consisting of three regular cells terminated with two RF couplers. Fig. 4 shows that the major contribution to the quadrupolar kick acting on the beam comes from the regions of the RF couplers, while no field asymmetry appears in the regular cells.

The racetrack parameters d, a and r are adjusted to obtain a reflection coefficient s_{11} at the input port of the coupler lower than -30 dB: couplers' geometric parameters have been tuned to match into the traveling wave structure varying the number of regular cells in between the two couplers [8]. Using this technique, results are not affected by the standing wave component.

Fig. 5 shows the value of k_q as a function of the racetrack parameter d. In our case, the integration line extends from the entrance of the beam-pipe up to the end of the first regular cell. Note that the minimum of k_q is reached for $d=13.5$ mm.

After optimizing the racetrack geometry in terms of the residual quadrupole component, the surface electric and magnetic fields have been evaluated assuming an input power of 65 MW. In the case of a 3-m long accelerating structure with a 10 mm iris radius, such a power is required to attain an overall accelerating gradient of 30 MV/m, quite demanding for an S-band accelerating structure.

As is evident from HFSS simulations (see Fig. 6), the axial electric field is slightly higher in the coupler region than in the regular cells for such a coupler.

Also, the surface electric field achieves its maximum value on the first beam iris (see Fig. 7), up to 93 MV/m. Of course, given the attenuation parameter for each cell, the field variation between

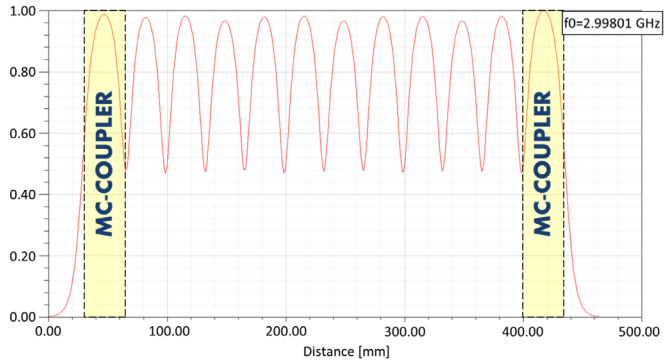

Fig. 6. Axial electric field E_z for a 10 cells accelerating structure.

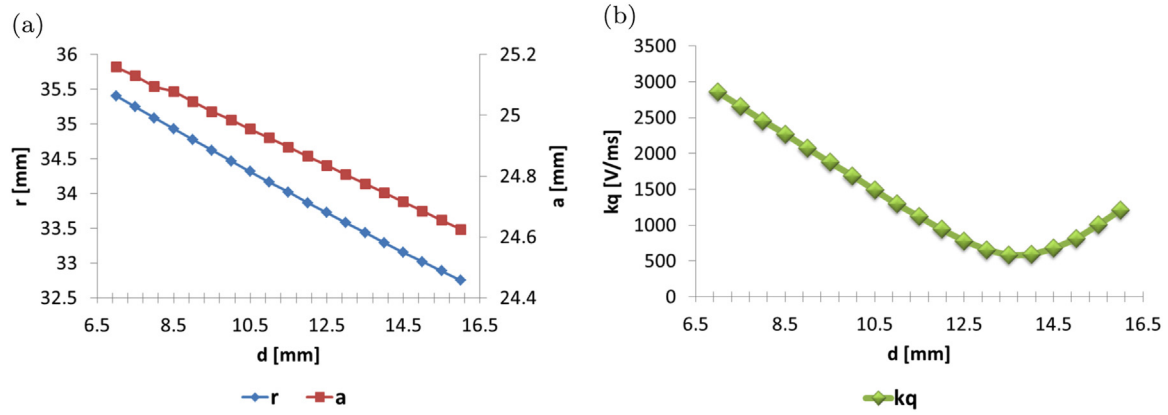

Fig. 5. Parameters of an MC-Coupler as a function of the racetrack parameter, (a) Slot Aperture a and Coupler Cell Radius r vs Racetrack Parameter d (b) k_q vs Racetrack Parameter d.

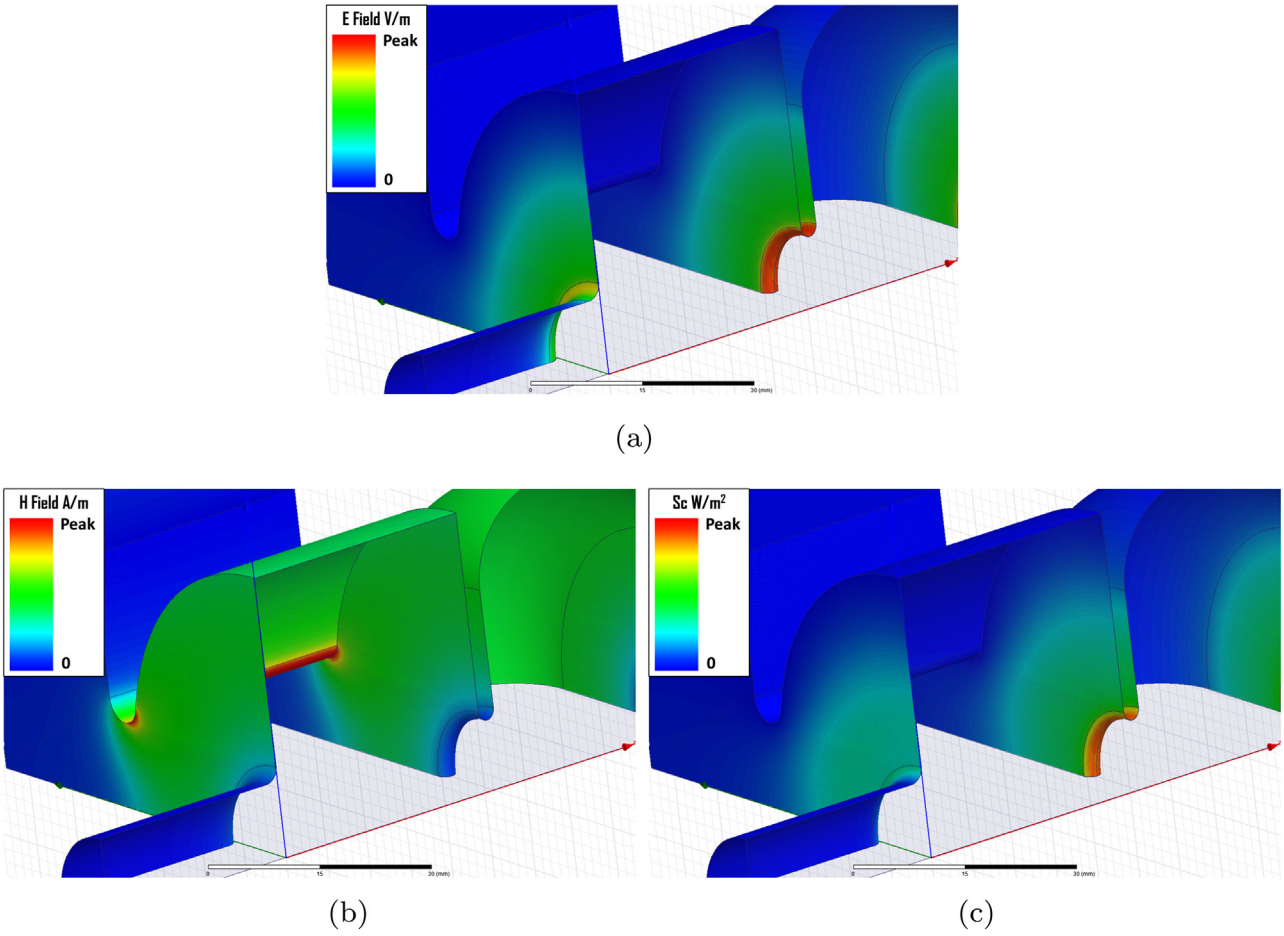

Fig. 7. Surface fields for an MC-coupler: (a) surface electric field, (b) surface magnetic field, (c) modified Poynting vector.

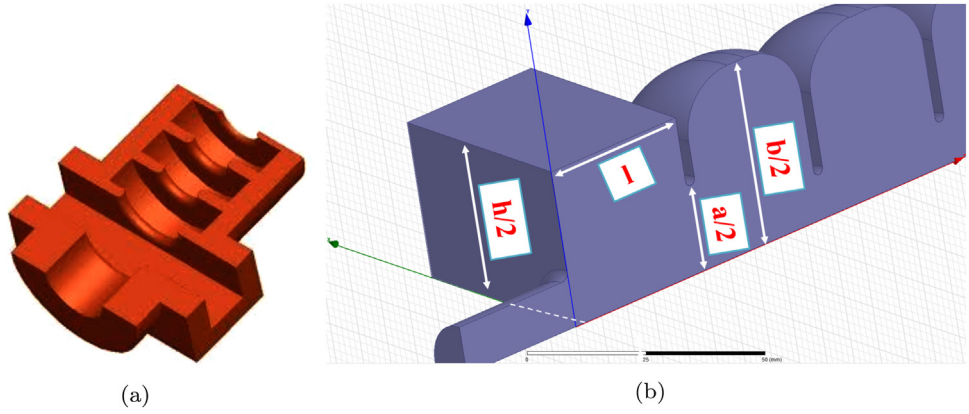

Fig. 8. Layout of a waveguide coupler:h is the length of the waveguide broad wall, l is the length of the waveguide narrow wall, a is the diameter of the beam iris and b is the outer diameter of the matching cell: (a) cut of an EC-coupler, (b) geometrical parameters of an EC-coupler.

one cell and the next one is rather small, less than 1%.

The surface magnetic field reaches its maximum value in the coupling slot region. By smoothing all the sharp edges connecting the waveguide to the coupler cell, it is possible to get a surface magnetic field H_{surf} as low as 175 kA/m, thus reducing the possible detrimental effects due to the pulse heating phenomena.

Limitations coming from RF breakdown in vacuum strongly influence the design of high gradient accelerating structures. In the framework of the CLIC (Compact LInear Collider) study [17] a significant effort has been made to derive a quantity to be used as a guide in the high gradient accelerating structure design and to perform quantitative performance predictions for accelerating structures.

In [18], the ratio P/C of the input power to the iris circumference has been proposed as a parameter which limits the achievable gradient in traveling wave structures. Nevertheless, because of some shortcomings which limit its applicability, a new local field quantity has been introduced [19] to evaluate the high gradient performance limit of accelerating structures in the presence of vacuum RF breakdown. This quantity is the so-called modified Poynting vector, given by the following expression [19]:

$$S_c = \left|\Re\left\{\vec{S}\right\}\right| + g_c\left|\Im\left\{\vec{S}\right\}\right| \tag{7}$$

The real part $\Re\left\{\vec{S}\right\}$ of the Poynting vector $\vec{S}=\frac{1}{2}\vec{E}\times\vec{H}^{*}$ describes the active power surface density in a traveling wave structure; g_c is a weighting factor and the imaginary part $\Im\left\{\vec{S}\right\}$ represents instead the reactive power surface density, related to energy oscillations, on each cycle, back and forth from the region of the electric field to the region of the magnetic field.

According to the simulation results, for such an RF coupler the maximum value of $|S_c|$ is nearly 0.7 W/μm^2. Considering the experimental data, this value of S_c results in a breakdown rate (i.e. number of breakdowns per pulse per meter, measured in bpp/m) of nearly 10^{-12} bpp/m if operating with an RF pulse of 700 ns and a gradient of 30 MV/m.

4. Electric-coupled RF coupler

Magnetic couplers presented above have been widely studied and used in accelerator design. Nevertheless, in the development of high gradient accelerating structures, the high electromagnetic fields arising in magnetic-coupled couplers could indeed represent a bottleneck. To remove possible limitations to the achievable operating gradients, novel changes in the couplers'design have been introduced: in [7,8], and different solutions have been studied in depth. Among all the modifications explored, waveguide couplers showed a clear and significant reduction of coupler surfaces fields.

As clearly explained in [7,8], for a waveguide coupler the input power coming from the source is directly coupled to the accelerator through a circular iris in the broad wall of the WR284 waveguide. The electric coupling requires a matching cell to match the input waveguide to the periodic structure (see Fig. 8).

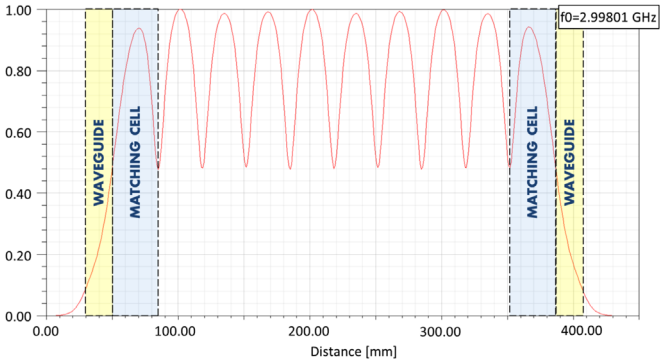

Fig. 9. Axial electric field E_z for the considered 10 cells accelerating structure.

In the following analysis, the performances for an EC-coupler both in terms of accelerating efficiency, residual quadrupole kick and electromagnetic surface fields will be presented. A comparison between the MC and EC couplers will be provided in the final section.

As can be seen from Fig. 9, the waveguide coupler (EC-coupler) sacrifices some acceleration efficiency. In the waveguide region the E_z field component is very low (see Fig. 9 where a 10 cells accelerating structure has been considered). Furthermore, in the matching cell the field may not be properly phased with the following accelerating cells. In our case, the accelerating efficiency has been partially improved by stepping down the narrow size l of the WR284 rectangular waveguide to 60% of its original length.

The value of the residual quadrupole component k_q, evaluated according to Eq. (6), has been then calculated by considering the exponential factor $e^{+j\frac{\omega}{c}z}$ and an integration line that extends from the entrance of the beam-pipe up to the end of the matching cell.

For a standard WR284 input waveguide, the resulting k_q is high if compared to the residual head–tail kick achievable with an optimized MC-coupler. To further improve the performance of the EC-coupler, an analysis has been performed with HFSS varying the geometric parameter h. For each value of the parameter h, the optimal values of a and b have been found in order to guarantee a value of the $|s_{11}|$ lower than -30 dB.

As illustrated in Fig. 10, by tuning the length of the waveguide broad wall h, the residual quadrupole strength k_q can be slightly reduced. The optimal value is attained when h is approximately equal to 100 mm. Nonetheless, such a value is still nearly four times the optimal value that could be attained with an optimized MC-coupler.

The surface fields, as well as the modified Poynting vector, have also been evaluated in the EC-coupler for an input power of 65 MW.

The surface electric field has its maximum value, of about 81 MV/m, on the first beam iris. Also, as illustrated in Fig. 11, the surface magnetic field H_{surf} in the coupler region is much lower than the one in the following cells where the maximum value is about 78 kA/m.

Considering that for the previously considered MC-coupler the surface magnetic field in the coupling slot region was approximately 175 kA/m, it is pretty evident that the limitations to high gradient operation due to RF pulse heating phenomena can be easily reduced.

Also, the value of the modified Poynting vector is a bit lower compared to the one obtained for an MC-coupler. For our EC-coupler, the maximum value of $|S_c|$ is in fact nearly 0.57 W/μm^2. Based on experimental evidence, this results in a breakdown rate probability of approximately 10^{-12} bpp/m if operating with an RF pulse of 700 ns.

In the next section all the relevant collected data concerning the MC-coupler and the EC-coupler will be summarized and some

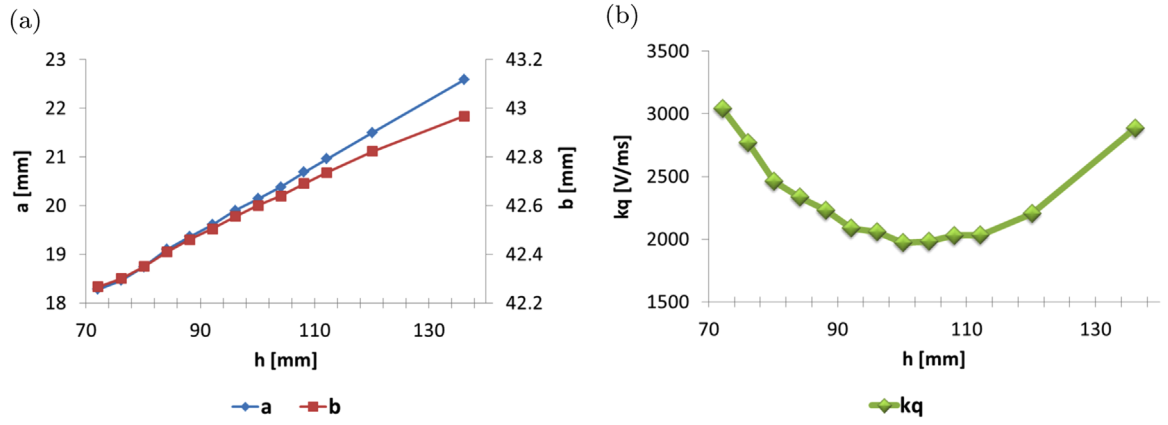

Fig. 10. Parameters of an EC-Coupler as a function of the waveguide width: (a) slot aperture a and coupler cell radius r vs waveguide width h, (b) k_q vs waveguide width h.

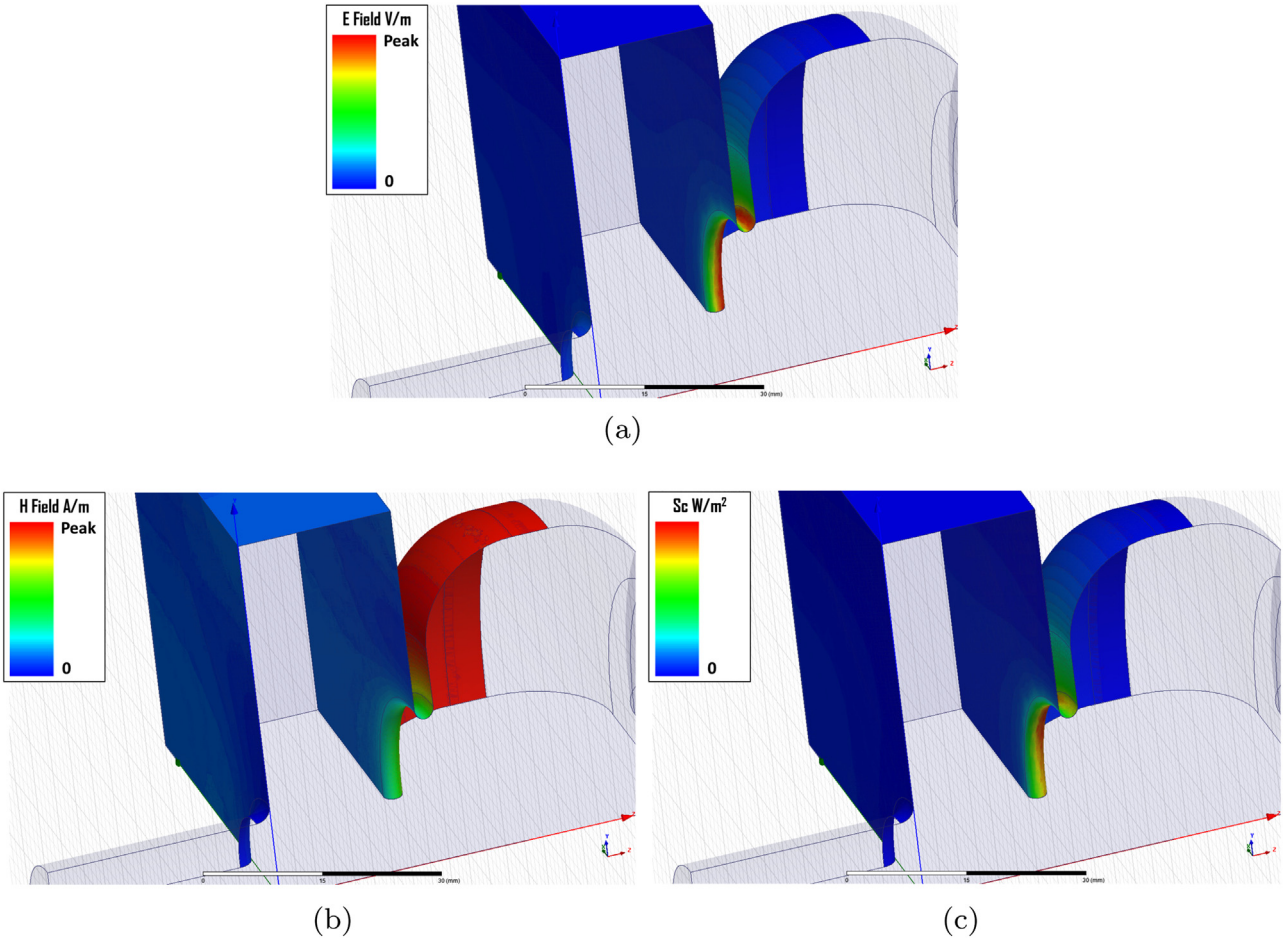

Fig. 11. Surface fields for an EC-coupler: (a) surface electric field, (b) surface magnetic field, (c) modified Poynting vector.

Table 1
Summary of RF parameters for both Electric Coupled and Magnetic Coupled RF couplers. All the field values are calculated for 65 MW of input power.

Couplers' type	E_{surf} (MV/m)	H_{surf} (kA/m)	S_c (W/μm^2)	k_q (V/ms)	Pros	Cons
MC couplers	93	175	0.7	582	Lower residual quadrupole field components Acceleration efficiency	High magnetic field at the coupling slot
EC couplers	81	78	0.57	1973	Very low surface magnetic field Easy to machine Cost reduction	Higher residual quadrupole field components Slightly reduced acceleration efficiency

remarks on advantages and disadvantages of the previously mentioned solutions will be described.

5. Conclusion

FERMI is a seeded free-electron laser, operating in the VUV to soft X-rays range. As a user machine, reliability has to be guaranteed even when the FEL is operated at its ultimate limit. In order to improve the current reliability while operating at full energy with a repetition rate of 50 Hz, a plan for replacing the existing S-band, BTW accelerating structures is under consideration. To get the desired performances, great care must be put into the designing of the new RF couplers. In this paper, two different solutions have been optimized and RF performances have been then compared.

One way of coupling the power to a TM_{01} mode is by using iris apertures located between the end wall of the rectangular waveguides and the coupling cell. As seen in Section 3 such a dual feed magnetic-coupled rf coupler has a residual quadrupole field component that can be minimized by using a racetrack profile in the coupler cell. Nonetheless, high surface magnetic fields in the proximity of the coupling slots can represent a bottleneck, due to the enhancement of the surface magnetic field in proximity of the coupling slots, for high gradient operation.

In [8], a novel change in the geometry of the rf coupler has been proposed to overcome this limitation. To do this a direct electric coupling into a matching cell through a circular iris in the waveguide broad wall has been implemented. In Section 4, the electric-coupled solution has been studied and numerical simulations have been performed to obtain surface fields and residual quadrupole components. All the data are then summarized in Table 1 and compared with the performances of a magnetic-coupled RF coupler.

As can be seen in Table 1, magnetic-coupled and electric-coupled RF couplers show similar values for S_c and the expected

breakdown rate as well. Consequently both the options meet the requirements for high gradient operation. Indeed, fabrication processes (surface finishing, cleaning procedures, etc.) could be a limiting factor, dramatically reducing the expected RF performances. For this reason, even if the expected breakdown rates are very similar, in practical cases solutions where peak surface fields are lower are preferred. EC-couplers show a significant reduction of the magnetic surface fields and therefore no limitation would arise due to field enhancement or rf pulse heating.

Nonetheless, a drawback of EC-couplers is in general a reduction of the acceleration efficiency. Even stepping down the narrow size of the WR284 rectangular waveguide, the acceleration efficiency in the coupler region for a particle traveling on-crest is reduced by about 40% compared to the MC-coupler. Of course, considering the whole length of the structure, the total energy loss over 3 m is less than 1% and can generally be more than compensated by allowing slightly higher power/gradient operation in the rest of the structure without reaching any breakdown limitations.

High frequency simulations show that the residual quadrupole field component is not as low as in the MC-coupler case. This makes the EC-coupler more suitable for use in the high energy part of a linear accelerator, where the e-beam is already compressed and its longitudinal momentum is high enough to not be affected by the quadrupolar kicks coming from the couplers' region.

The final decision about the most appropriate solution will be made based on further criteria such as cost. For example the mechanical simplicity of EC-couplers makes them easy to machine with a significant cost reduction that could have a non-negligible impact on the whole project.

Acknowledgments

The authors acknowledge Walter Wuensch for his careful reading and editing of the paper.

References

[1] B.W.J. McNeil, N.R. Thompson, X-ray free-electron lasers, Nat. Photon. 4 (2010) 814.
[2] E. Allaria, et al., Two-stage seeded soft-x-ray free-electron laser, Nat. Photon. 7 (2013) 913.
[3] E. Allaria et al., Two-colour pumpprobe experiments with a twinpulse-seed extreme ultraviolet free-electron laser, Nat. Commun. 4, 2476.
[4] G. Penco et al., Experimental demonstration of electron longitudinal phase space linearization by shaping the photoinjector laser pulse, Phys. Rev. Lett. 114, 013901.
[5] V.A. Dolgashev, High magnetic fields in couplers of x-band accelerating structures, in: Proceedings of the Particle Accelerator Conference, vol. 2, 2003, p. 1267.
[6] V.A. Dolgashev et al., Effect of rf parameters on breakdown limits in high-vacuum x-band structures, Slac-pub-10175, SLAC, 2003.
[7] S. Dobert et al., Coupler studies for clic accelerating structures, Clic-note-517, CERN, 2002.
[8] C. Nantista, et al., Low-field accelerator structure couplers and design technique, Phys. Rev. Special Top. Accel. Beams 7 (2004) 072001.
[9] P.K. Ambattu, et al., Coupler induced monopole component and its minimization in deflecting cavities, Phys. Rev. Special Top. Accel. Beams 16 (2013) 062001.
[10] Z. Li et al., On the importance of symmetrizing rf coupler fields for low emittance beams, Slac-pub-14436, SLAC, 2011.
[11] A. Grudiev, Radio frequency quadrupole for landau damping in accelerators, Phys. Rev. Special Top. Accel. Beams 17 (2014) 011001.
[12] G. Barranco et al., Study of mutipolar RF kicks from the main deflecting mode in compact crab cavities for LHC, in: Proceedings of IPAC2012, 2012, p. 1873.
[13] D. Alesini, Power coupling, Cern Accel. Sch. (2010).
[14] L. Xiao et al., Dual feed rf gun design for the LCLS, in: Proceedings of the Particle Accelerator Conference, 2005, p. 3432.
[15] Z. Li et al., Coupler design for the LCLS injector s-band structures, in: Contributed to the Particle Accelerator Conference, 2005, p. 2176.
[16] ANSYS HFSS, high frequency electromagnetic field simulation (2016). URL ⟨http://www.ansys.com/Products/Electronics/ANSYS-HFSS⟩.
[17] Clic-note-764, CERN, 2008.
[18] W. Wuensch, Clic-note-649, CERN, 2006.
[19] A. Grudiev, et al., New local field quantity describing the high gradient limit of accelerating structures, Phys. Rev. Special Top. Accel. Beams 12 (2009) 102001.